A New Projection Space for Separation of Specular-Diffuse Reflection Components in Color Images

Jianwei Yang[1], Zhaowei Cai[1], Longyin Wen[1], Zhen Lei[1]
Guodong Guo[3], Stan Z. Li[1,2⋆]

[1]CBSR & NLPR, Institute of Automation, Chinese Academy of Sciences, China
[2] China Research and Development Center for Internet of Thing
[3] Dept. of Computer Science and Electrical Engineering, West Virginia University
[1,2]{jwyang, zwcai, lywen, zlei, szli}@cbsr.ia.ac.cn; [3]gdguo@cs.wisc.edu

Abstract. In this paper, we propose a new reflectance separation model to separate the diffuse and specular reflection components. The model is based on a two-dimensional space called Ch-CV space, which is spanned by maximum chromaticity and the coefficient of variation (CV) of RGB color. The space exhibits a more direct correspondence to diffuse and specular reflection components than the RGB color space, as well as the HSI color space. Under the whitened illumination, the surface points with the same diffuse chromaticity have the same slope in Ch-CV space. Based on these properties, we propose a slope-based region growing method to implement an image segmentation in the specular regions, and to separate the reflection components for each segmented region. The comparison experiments with several state-of-the-art algorithms show its superior capability to separate the specular and diffuse reflection components.

1 Introduction

In recent years, separating the diffuse and specular reflection components in color images has become an important research topic. Lots of highlight detection and removal methods have been proposed. In these method, the dichromatic reflectance model [1] has been widely utilized with the assumption that the reflected light can be separated into specular and diffuse reflections, respectively.

In terms of the quantity of input data, the reflection component separation algorithms can be categorized into two groups [2]: multi-image based and single-image based methods. In the early multi-image based methods, polarization method was introduced in conjunction with color information [3–5]. Later, Sato and Ikeuchi [6] introduced a temporal-color space to analyze the diffuse and specular reflections based on colors and image intensity. Lin and Shum [7,8] changed the light source direction to produce two photometric images and used linear basis functions to separate the specular components. Based on the observation that the shift of the highlights in sequential images is generated by

⋆ Corresponding author.

the shift of the light source, Feris et al. [9] proposed a multi-flash method. In addition, [10] and [11] also use multiple images to separate specular and diffuse reflection components. However, multiple images are not always available under many circumstances in practice.

Many reflection separation methods which rely on a single image have been proposed. Klinker [12] extended the dichromatic model by introducing a T-shaped color space. In this model, the diffuse component of highlight is estimated through projecting the highlight limb to the diffuse one. However, this T-shaped distribution will degrade much in image areas with uniform hue but various saturation. Alternatively, Bajscy et al. [13] proposed a specified three-dimensional space called S space. However, to construct S_0 axis of S space, they must use a spectro-photometer to measure the scene radiance, which is not practical in many cases. Different from the previous works, Mallick et al. proposed a data-driven color space called SUV space [14]. In this space, the specular and diffuse components are separated into S channel and UV channel, then the highlights are removed by iteratively eroding the specular channel using either a single image or video sequences [15]. Actually, when the input image is under whitened illumination, all the analysis in the SUV space can be turned to RGB space. Therefore, it is also vulnerable to a multi-colored or textured images.

Different from the previous approaches which are based on three-dimensional space, Tan and Ikeuchi [16] proposed a novel mechanism based on a two-dimensional Maximum Chromaticity-Intensity space. In their method, the diffuse component is obtained by locally iterative calculation based on a specular-free (SF) image for each pixel. Unfortunately, though no prior image segmentation is needed, this method leads to a much higher computational complexity and much color distortions in image, especially at edge areas. Considering the computational complexity, Yang et al. [17] exploited a fast bilateral filtering technique. This method estimates the maximum diffuse chromaticity by directly applying low-pass filter. However, it results in much more color distortions at edges, as well as inside the region of uniform color. On the other hand, Yoon et al. [18] also proposed an iterative framework based on the comparison of local ratios. A modified specular-free (MSF) image was introduced, the reflection components were achieved by comparing local ratios between input and MSF images, followed by making those ratios equal in an iterative framework. The MSF image was also exploited in the work of Shen et al. [19, 20]. Unfortunately, the type of methods based on MSF image may wrongly estimate the reflection components due to color discontinuities in surface edge regions.

In this paper, we exploit a two-dimensional space called Ch-CV space to separate the reflection components in a single image, the space which is spanned by the maximum chromaticity and the coefficient of variation of color intensity. There are three major properties about the proposed space: i) under the whitened illumination, the Ch-CV space provides a linear description of the specular and diffuse reflections; ii) the polar coordinate values exhibit a more direct relationship to reflection components; iii) there is a one-to-one correspondence between HSI color values and the polar coordinate values in Ch-CV space: the

surface with identical hue and saturation also has identical characteristics in Ch-CV space.

As mentioned before, Tan et al. [16] also proposed a two-dimensional space called Maximum Chromaticity-Intensity space so that the separation can be described as a closed-from. However, the non-linearity of their space leads to the necessariness of an iterative algorithm to removal the highlights in an image. In contrast, the Ch-CV space provide a linear description of the specular and diffuse reflections, which can avoid the iterative estimation process [16, 18]. Based on its properties, we propose a region growing method to segment specular regions, and then obtain the maximum diffuse chromaticity for each segmented region. In this way, the interferences among neighboring surfaces of various color in the previous work are avoided in our method. As a result, the separation results are more reliable and accurate than those in previous works.

2 Surface Reflection Model

Based on the dichromatic reflection model [1], the color intensity of pixels in an image can be computed by the integration over the light spectrum as follows:

$$I_c(x) = \omega_d(x) \int \tau_c(\lambda) S_d(\lambda, x) E(\lambda) d\lambda + \omega_s(x) \int \tau_c(\lambda) S_s(\lambda, x) E(\lambda) d\lambda \tag{1}$$

where $S_d(\lambda, x)$ and $S_s(\lambda, x)$ are the spectral distribution function of diffuse reflection and specular reflection, respectively; $E(\lambda)$ is the spectral power distribution of illumination light (assume there is a single light source); $\tau_c(\lambda)$ is the transmittance function of the camera sensor, and the subscript $c \in \{r, g, b\}$, representing three color channels: red, green and blue; $\omega_d(x)$ and $\omega_s(x)$ are the geometric scale factors of diffuse reflection and specular reflection, respectively, which merely depend on the geometry of a surface point.

We define the diffuse chromaticity $\boldsymbol{\Lambda} = \{\Lambda_r, \Lambda_g, \Lambda_b\}$ and specular chromaticity $\boldsymbol{\Gamma} = \{\Gamma_r, \Gamma_g, \Gamma_b\}$ as those in [16]. For each channel, $\Lambda_c(x) = J_c^d / \sum_c J_c^d$, and $\Gamma_c = J_c^s / \sum_c J_c^s$. Here, $J_c^d = \int \tau_c(\lambda) S_d(\lambda, x) E(\lambda) d\lambda$ and $J_c^s = \int \tau_c(\lambda) S_s(\lambda, x) E(\lambda) d\lambda$. Then the color intensity of pixels for each channel $c \in \{r, g, b\}$ becomes:

$$I_c(x) = m_d(x) \Lambda_c(x) + m_s(x) \Gamma_c \tag{2}$$

As explained in [16], both the sum of diffuse chromaticity vector $\boldsymbol{\Lambda}$ and that of specular chromaticity vector $\boldsymbol{\Gamma}$ are equal to 1, that is, $\sum_c \Lambda_c = \sum_c \Gamma_c = 1$. As a result, the sum of color intensity will be $\sum_c I_c(x) = m_d(x) + m_s(x)$.

3 The Proposed Reflection Separation Model

3.1 Illumination Chromaticity Normalization

In the real world, most illumination light are not pure white because of the non-uniform spectral distribution of light source and different transmittance function

of camera sensors. In this paper, we utilize the normalization approach introduced in [21] to obtain a normalized specular-diffuse color image, which is derived by dividing the estimated illumination chromaticity in both sides of Eq. (2):

$$I'_c(x) = m'_d(x)\Lambda'_c(x) + m'_s(x)\Gamma'_c = m'_d(x)\Lambda'_c(x) + \frac{m'_s(x)}{3} \tag{3}$$

where $m'_d(x) = m_d(x)\sum_c \frac{\Lambda_c(x)}{\Gamma_c^e}$, $m'_s(x) = 3m_s(x)$. Obviously, the sum of $\boldsymbol{\Lambda'}$ is still equal to 1, and the same to $\boldsymbol{\Gamma'} = \{\frac{1}{3}, \frac{1}{3}, \frac{1}{3}\}$. Upon the completion of normalization, the reflection separation can be conducted to achieve the normalized reflection components, followed by transferring the components to the previous un-normalized components [16].

3.2 The Illustration of Ch-CV Space

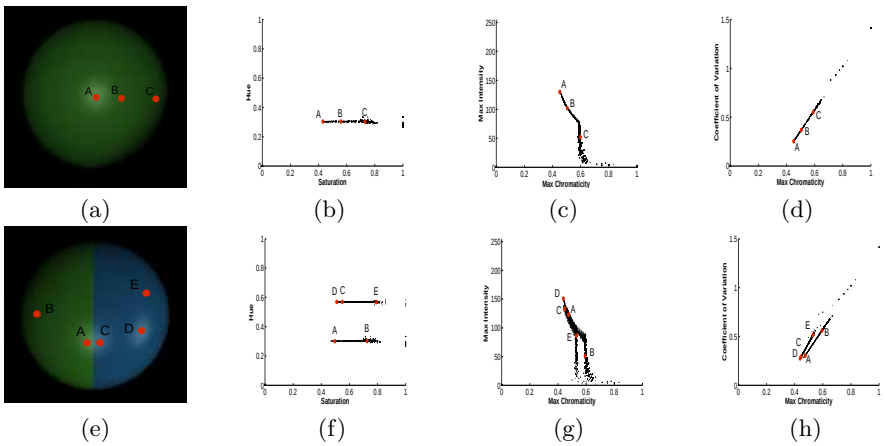

Fig. 1. Projections of single-colored image and bi-colored image into the three spaces. (a) and (e): Synthetic *green ball* and synthetic *blue-green ball*. (b) and (f): Projection of images into Hue-Saturation space. (c) and (g): Projection of images into Maximum Chromaticity-Intensity space. (d) and (h): Projection of images into Ch-CV space.

In this part, by comparing the Ch-CV space with the Maximum Chromaticity-Intensity space [16] and HSI color space [22], we demonstrate the claimed properties of Ch-CV space. At first, we explain the linearity in Ch-CV space.

Given a normalized input image, the maximum chromaticity is defined as:

$$\sigma(x) = \frac{\max(I'_r(x), I'_g(x), I'_b(x))}{\sum_c I'_c(x)} \tag{4}$$

The coefficient of variation (CV), which is defined as the ratio of the standard deviation to the mean of color intensity $\boldsymbol{I} = \{I'_r, I'_g, I'_b\}$ in a normalized image,

is with the following formulation:

$$CV(x) = \frac{\sqrt{\frac{1}{3}\sum_c (I'_c(x) - I'_m(x))^2}}{I'_m(x)} \tag{5}$$

where $I'_m(x)$ is the mean of RGB color. According to Eqs. (3), (4) and (5), all of the specular only points locate exactly at $(1/3, 0)$ in the Ch-CV space because their color intensity $I'(x) = \{\frac{m'_s(x)}{3}, \frac{m'_s(x)}{3}, \frac{m'_s(x)}{3}\}, m'_s(x) \neq 0$. We regard the point $(1/3, 0)$ as the origin in the following analysis.

Substituting Eq. (3) into Eq. (5), the CV of surface point x has the following formulation:

$$CV(x) = \frac{\sqrt{3\sum_c I'^2_c(x) - (\sum_c I'_c(x))^2}}{m'_d(x)(\max_c \Lambda'_c - \frac{1}{3})}(\sigma(x) - \frac{1}{3}) \tag{6}$$

In Eq. (6), if the fraction at the right side is a constant, then the CV will be linear with the maximum chromaticity σ. In other word, the distribution of transformed RGB image in the Ch-CV space assembles a sector which consists of a cluster of straight lines with different slopes. In addition, these lines will exactly intersect at the specular only point $(1/3, 0)$ if ruling out the absolute black points. In the following analysis, the absolute black surface points are filtered out.

According to Eq. (6), for each surface point x in a normalized image, its slope is described as:

$$k(x) = \frac{\sqrt{3\sum_c I'^2_c(x) - (\sum_c I'_c(x))^2}}{m'_d(x)(\max_c \Lambda'_c - \frac{1}{3})} \tag{7}$$

Furthermore, based on Eq. (3), the slope of surface point x can be simplified to be:

$$k(x) = \frac{\sqrt{3\sum_c \Lambda'^2_c(x) - 1}}{(\max_c \Lambda'_c(x) - \frac{1}{3})} \tag{8}$$

Eq. (8) explains that the slopes of surface points in the Ch-CV space are merely determined by their diffuse chromaticities; therefore, the surface points that have the same diffuse chromaticity will have identical slope in the Ch-CV space. Meanwhile, the range of slope is exactly $[3\sqrt{2}/2, 3\sqrt{2}]$, where $3\sqrt{2}/2$ and $3\sqrt{2}$ correspond to the case that one component of $\boldsymbol{\Lambda'}$ is equal to 1 and the case that two components of $\boldsymbol{\Lambda'}$ are equal to 0.5, respectively. Clearly, the permutation of the values of $\boldsymbol{\Lambda'}$ among RGB channels will result in the same slope. To avoid the confusions among three channels, we split the original space into six sub-spaces according to the relationship of RGB value. From the last column in Fig. 1, we can find the projection of the normalized *green ball* in the Ch-CV space composes a single straight line, and there are two principal lines for the normalized *blue-green ball*. It should be noted that we present only one Ch-CV sub-space rather than all the six ones since there is no overlapped lines in the space.

Another property of Ch-CV space is that there exist one-to-one correspondence between the HSI color values and the polar coordinate values in Ch-CV

space. The surface points with identical hues also have identical slopes in Ch-CV space, and the saturation corresponds to the horizonal coordinate as well as polar radius .

Based on the Eq. (3), the hue of surface point in normalized image is reformulated as:

$$H(x) = cos^{-1}[\frac{3\sqrt{2}}{2}\frac{\Lambda'_r(x) - \frac{1}{3}}{\sqrt{3\sum_c \Lambda'^2_c(x) - 1}}] \tag{9}$$

Comparing Eq. (8) with Eq. (9), we can find the slope in Ch-CV space corresponds to the hue component of HSI color. Therefore, the surface points with the same diffuse chromaticity $\boldsymbol{\Lambda'}$ have not only the same slope in Ch-CV space, but also the same hue in HSI space. Comparing the second and forth columns in Fig. 1, we can see that the surface points with identical hue construct a slant straight line in the Ch-CV space.

Though the level of specular component is irrelevant to the slope in the Ch-CV space (or hue in HSI space), it does decide the surface points' location in a single line. By constituting Eq. (3) into Eq. (4), the maximum chromaticity for each surface point can be written as:

$$\sigma(x) = \frac{m'_d(x)\max_c \Lambda'_c(x) + \frac{1}{3}m'_s(x)}{m'_d(x) + m'_s(x)} \tag{10}$$

Clearly, $\sigma(x)$ is equal to $1/3$ when $m'_d(x) = 0$, and it is equal to $\max_c \Lambda'_c(x)$ when $m'_s(x) = 0$. In other word, given a color surface with a certain $\boldsymbol{\Lambda'}$, $\max_c \Lambda'_c = \sigma$ for the diffuse only points. More generally, in a homogeneous color surface, the larger the specular component is, the smaller σ is. Actually, the distribution of a homogeneous color surface in the Ch-CV space is a segmented line, which starts from $(1/3, 0)$ and ends at the point $(max_c\Lambda'_c, \sqrt{3\sum_c \Lambda'_c - 1})$. Consequently, as for a uniform color image, there is only one segmented line with a certain slope, whereas for a multi-colored image, there may exist several overlapped segmented lines with the same slope in the Ch-CV space, and each of them corresponds to an unique diffuse chromaticity $\boldsymbol{\Lambda'}$, in spite of their same slopes.

The above analysis indicates that the maximum chromaticity σ also represents a characteristic of surface color, which is analogous to the saturation value in HSI color space. Specifically, the suturation is formulated as follows:

$$S = 1 - (\frac{3}{I'_r + I'_g + I'_b})\min_c I'_c \tag{11}$$

Substituting I'_c in Eq. (3) into Eq. (11), we have:

$$S(x) = \frac{m'_d(x)}{m'_d(x) + m'_s(x)}(1 - 3\min_c \Lambda'_c(x)) \tag{12}$$

Meanwhile, the maximum chromaticity for point x can be re-formulated as:

$$\sigma(x) = \frac{1}{3} + \frac{m'_d(x)}{m'_d(x) + m'_s(x)}(\max_c \Lambda'_c(x) - \frac{1}{3}) \tag{13}$$

According to the last two equations, given a group of surface points with identical diffuse chromaticity $\boldsymbol{\Lambda'}$, both S and σ are maximized by the diffuse only

points ($m'_s = 0$), and their values are $(1 - 3\min_c \Lambda'_c)$ and $\max_c \Lambda'_c$, respectively. Moreover, by combining Eq. (8) and the normalization condition of $\boldsymbol{\Lambda'}$, we will obtain the unique solution of $\min_c \Lambda'_c$ if given the value of $\max_c \Lambda'$, and versa vice. Therefore, the surface points with the same hue and saturation will also have the same slope and maximum chromaticity in Ch-CV space. This relationship also holds between saturation and the polar radius in Ch-CV space. The labeled points in Fig. 1 proves our numerical analysis.

At this point, we have proved the claimed properties of the Ch-CV space. Though similar to HSI color space, there is a crucial difference between such two spaces. In HSI space, m'_d, a vital intermediate factor for reflection separation, cannot be derived from the hue formula given the $\min_c \Lambda'_c$ in Eq. (12), whereas it is computable in Eq. (7) if the value of $\max_c \Lambda'_c$ is obtained from Eq. (13). Another property of the Ch-CV space is that we can achieve maximum diffuse chromaticity and $m'_d(x)$ directly by making use of the linearity in Ch-CV space. Therefore, as for the reflection separation task based on dichromatic reflectance model, the Ch-CV space is superior than the aforementioned spaces, including S space, Maximum Chromaticity-Intensity space and HSV color space.

4 Specular-Diffuse Reflection Components Separation

This section will focus on how to separate specular and diffuse reflection components based on Ch-CV space. According to Eq. (3), given a normalized image, to separate the reflection components means to decompose the color intensity into two partitions, $m'_d(x)\Lambda'_c(x)$ and $\frac{1}{3}m'_s(x)$ for each color channel $c \in \{r, g, b\}$ in specular regions.

Before the separation, we choose the specularity detection method presented in [20] to determine the specular surface points in an image. Similarly, we dilate the original detected specular region into a larger one containing both specular and diffuse surface points in general case, and we call such regions diffuse-specular connected regions. To separate the reflection components in the specular regions, we first transform the normalized image into the Ch-CV space. According to Eq. (7), $m'_d(x)$ can be written as:

$$m'_d(x) = \frac{\sqrt{3\sum_c I'^2_c(x) - (\sum_c I'_c(x))^2}}{k(x)(\max_c \Lambda'_c(x) - \frac{1}{3})} \tag{14}$$

Eq. (14) illustrates that $m'_d(x)$ can be derived for every surface point given its slope and maximum diffuse chromaticity among thee color channels. Therefore, the derivation of m'_d can be divided into two stages: a) obtain $k(x)$; b) decide the $\max_c \Lambda'_c(x)$ for the surface points.

In a normalized image, the slopes of specular surface points can be calculated simply by $CV(x)/(\sigma(x) - 1/3)$. After obtaining the slopes of specular surface points, we can determine their maximum diffuse chromaticity based on the proof that it is identical to the maximum chromaticity of the the diffuse only points with the same hue. However, there may be no diffuse only points for some surfaces in practice. In such case, we can regard the points with the maximum σ as the

diffuse only ones, which is rational due to the fact that we care more about removing the highlights in the input image, rather than getting an exactly diffuse only image. Unfortunately, there may exist diffuse surfaces with the same hue yet different saturation in a multi-colored image. In such case, the surface points having the same slope in a Ch-CV sub-space may correspond to distinctive $\boldsymbol{\Lambda'}$. As a result, we should estimate the corresponding diffuse chromaticity for each surface with various saturation in each line optimally, rather than assign the single value of maximum σ to the $\max_c \Lambda'_c$ of all the surface points in a line.

In this paper, we use a 8-connected region growing method [23] to segment the specular regions so that surface points in each segmented region have similar hue. In our algorithm, we define an uniformity parameter η for the segmentation, and we set it to be a constant value 0.12, which is suitable for most images. After conducting the algorithm, we can obtain all the connected regions with similar hue values (or slopes) within the constraint of uniformity parameter. In each connected region, we assume the surface points share the same diffuse chromaticity $\boldsymbol{\Lambda'}$. Inspired by [20], the smoothness of diffuse reflection component are considered in our algorithm. In each diffuse-specular connected regions, the optimal $\max_c \Lambda'_c$ can be obtained under the condition that the difference between the mean RGB color intensity diffuse component in the specular region and that of surrounding diffuse region is minimized. Based on the Least Square Error (LSE) algorithm, we can obtain the optimal $\max_c \Lambda'_c$ for each specular surface point, then m'_d can be calculated by Eq. (14), and m'_s can be calculated for each surface point by using the equation $m'_s(x) = \sum_c I'_c(x) - m'_d(x)$. Afterward, the diffuse component of surface points can be derived according

$$m'_d(x)\Lambda'_c(x) = I'_c(x) - \frac{m'_s(x)}{3}. \tag{15}$$

Furthermore, the diffuse chromaticity $\boldsymbol{\Lambda'}$ can be obtained by dividing the diffuse component by m'_d. Fig. 2 shows the derived components of image *head*.

In practice, it is probably that all of the surface points in a connected region are specular ones. In this case, we estimate their specular reflection component directly. Based on the continuity of specularity in an image, we determine m'_s for each specular surface point by calculating the mean value of specular components in its surrounding 5×5 neighborhood.

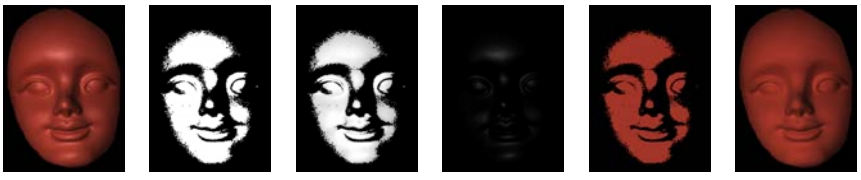

(a) (b) (c) (d) (e) (f)

Fig. 2. (a) Input image *head*. (b) Detected specular region. (c) m'_d, (d) m'_s and (e) $\boldsymbol{\Lambda'}$ in the specular region. (f) Diffuse component of *head*.

5 Experiments

The proposed method is compared with five previous methods [16–20]. In our experiments, 13 test images from previous works are used in our experiment, and two other images are synthesized to give a quantitative comparisons by using the PBRT v2.0 software [24]. All the experiments are performed on a PC with Intel Core i5, CPU 2.67 GHz, 2G RAM. Because of the limited space, we only present the better experimental results from Shen's two papers [19] and [20].

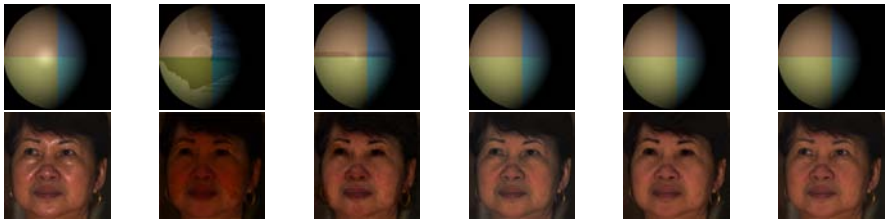

(a) (b) (c) (d) (e) (f)

Fig. 3. Comparison of diffuse components of *synth* and *lady*. Form left to right: (a) input images. (b) Diffuse components from [16]. (c) Diffuse components from [18]. (d) Diffuse components from [19, 20]. (e) Diffuse components from [17]. (f) Diffuse components from the proposed method.

In Fig. 3, we first use a synthetic image *synth* and a real-world image *lady* to evaluate the separation performance. Then two real-world images with multicolored and textured surfaces are used to compare the performance of five methods. Fig. 4 shows the diffuse components of real-world input image *fish* from five methods. As we can see, the diffuse component from the proposed method has the least color distortion, and the highlights in the image are removed effectively as well. In contrast, the method proposed by Tan et al. [16] fails to find the correct maximum diffuse chromaticity at color edges, leading to an obvious color distortions at edges. Moreover, because of its neighbor-based iteration algorithm, the original color distortion at edges spread inside. Though the method in [17] accelerates the separation process significantly by introducing inter-patch based algorithm rather than inter-pixel based, the result has much more color distortion than [16] because more color interferences between surfaces of different diffuse chromaticities are caused by inter-patch algorithm. The methods in [18–20] utilize a new specularity-invariant color image representation, MSF image. Yoon et al. [18] introduced an iteration scheme for neighboring pixels, which leads to much color distortions as well. To reduce the distortions, Shen et al. [19, 20] detect the highlight regions first, and then conduct local least-squares technique for each highlight region. However, though the results are acceptable in the specular regions of uniform color, the specular components are wrongly estimated in textured specular regions, such as the region around the eye of *fish* in Fig. 4d.

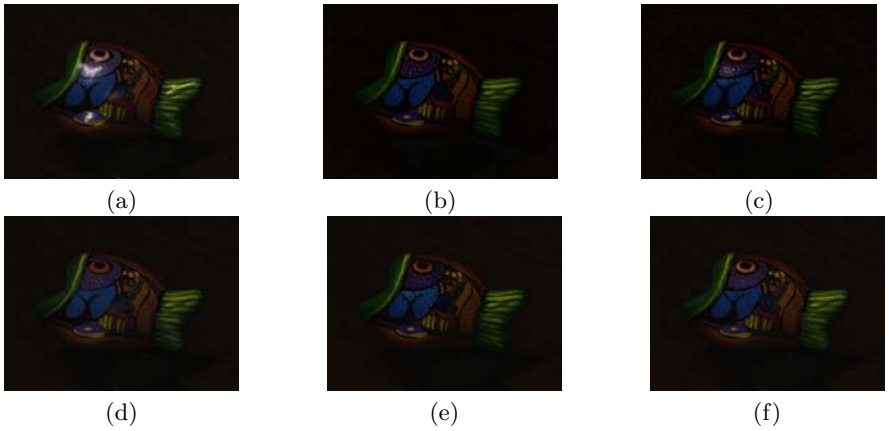

Fig. 4. (a) Input image *fish*. (b) Diffuse component from [16]. (c) Diffuse component from [18]. (d) Diffuse component from [19, 20]. (e) Diffuse component from [17]. (f) Diffuse component from the proposed method.

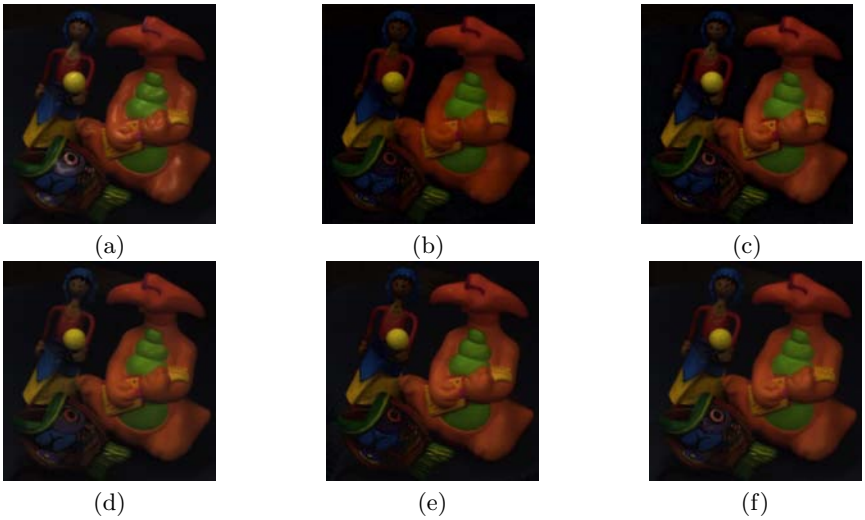

Fig. 5. (a) Input image *toys*. (b) Diffuse component from [16]. (c) Diffuse component from [18]. (d) Diffuse component from [19, 20]. (e) Diffuse component from [17]. (f) Diffuse component from the proposed method.

In comparison, the proposed method can obtain accurate and robust separate reflection components for images with both uniform color and highly textured specular regions. By introducing a reflectance separation model based on the Ch-CV space and region growing algorithm, we can derive accurate diffuse chromaticity for each connected region, and rule out the interferences among regions of different diffuse chromaticities. The diffuse component of another real world image *toys* presented in Fig. 5 also supports to our claim.

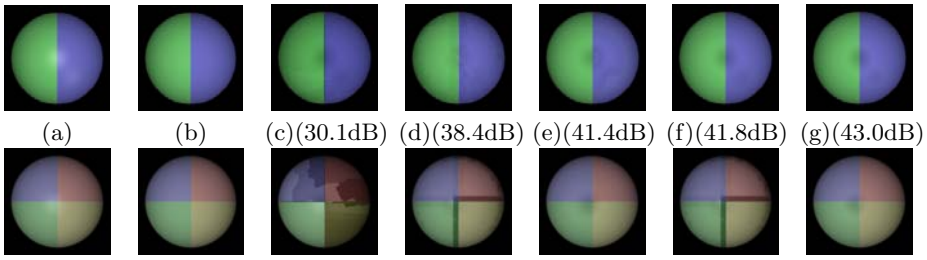

Fig. 6. Form left to right, the images are: input images, ground truth, diffuse components from [16], [18], [19,20], [17] and the proposed method. The corresponding PSNR value are reported below each image.

We adopt the peak signal-to-noise ratio (PSNR) to evaluate the methods quantitatively. The experiments are conducted on our self-synthesized images. As shown in Fig. 6, the proposed method achieves higher PSNR values than the other methods. Moreover, we compare computational cost of different methods. We compute the average time costs over all the test images: *ball-green*, *ball-blue-green*, *synth*, *head*, *pear*, *fish*, *toys*, *bear*, *bear2*, *red-pear*, *red-pear2*, *train*, *lady* and the other two self-synthesized images. The average time costs for all the methods are: 37.42s [16], 88.36s [18], 5.82s [19], 0.18s [20], 0.10s [17] and 6.25s (proposed). Because the proposed algorithm does not involve iterative process, the time cost is lower than the iterative methods [16, 18]. In our algorithm, the derivation of diffuse chromaticity should be conducted for each connected specular region, therefore, the time cost is comparable to [19], and higher than the methods in [17, 20].

6 Conclusion

In this paper, a new two-dimension space, called Ch-CV space is proposed. In the space, images are transformed to be a cluster of straight lines intersecting at a single point, leading to a fast and accurate derivation of the maximum diffuse chromaticity for all specular surfaces with various colors. Compared with the previous methods, the proposed one exploits a physical description of natural color, which facilitates the effectiveness of highlight removal in images, especially the multicolored and textured images. The further work will be focused on accelerating the reflection components separation process without additional color distortions.

Acknowledgement. This work was supported by the Chinese National Natural Science Foundation Project #61070146, #61105023, #61103156, #61105037, #61203267, National IoT R&D Project #2150510, Chinese Academy of Sciences Project No. KGZD-EW-102-2, European Union FP7 Project #257289 (TABULA RASA http://www.tabularasa-euproject.org), and AuthenMetric R&D Funds.

References

1. Shafer, S.: Using color to separate reflection components. Color Research and Applications **10** (1985) 210–218
2. Artusi, A., Banterle, F., Chetverikov, D.: A survey of specularity removal methods. Comput. Graph. Forum **30** (2011) 2208–2230
3. Wolff, L.B.: Polarization-based material classification from specular reflection. IEEE Trans. Pattern Anal. Mach. Intell. **12** (1990) 1059–1071
4. Wolff, L.B., Boult, T.E.: Constraining object features using a polarization reflectance model. IEEE Trans. Pattern Anal. Mach. Intell. **13** (1991) 635–657
5. Nayar, S.K., Fang, X.S., Boult, T.E.: Separation of reflection components using color and polarization. International Journal of Computer Vision **21** (1997) 163–186
6. Y, S., K, I.: Temporal-color space analysis of reflection. JOSA **11** (1994) 2990–3002
7. Lin, S., Shum, H.Y.: Separation of diffuse and specular reflection in color images. In: CVPR (1). (2001) 341–346
8. Lin, S., Li, Y., Kang, S.B., Tong, X., Shum, H.Y.: Diffuse-specular separation and depth recovery from image sequences. In: ECCV (3). (2002) 210–224
9. Feris, R., Raskar, R., Tan, K.H., Turk, M.: Specular reflection reduction with multi-flash imaging. In: SIBGRAPI. (2004) 316–321
10. Umeyama, S., Godin, G.: Separation of diffuse and specular components of surface reflection by use of polarization and statistical analysis of images. IEEE Trans. Pattern Anal. Mach. Intell. **26** (2004) 639–647
11. Chen, T., Goesele, M., Seidel, H.P.: Mesostructure from specularity. In: CVPR (2). (2006) 1825–1832
12. Klinker, G., Shafer, S.A., Kanade, T.: The measurement of highlights in color images. International Journal of Computer Vision **2** (1988) 7–32
13. Bajcsy, R., Lee, S.W., Leonardis, A.: Detection of diffuse and specular interface reflections and inter-reflections by color image segmentation. International Journal of Computer Vision **17** (1996) 241–272
14. Mallick, S.P., Zickler, T., Kriegman, D.J., Belhumeur, P.N.: Beyond lambert: Reconstructing specular surfaces using color. In: CVPR (2). (2005) 619–626
15. Mallick, S.P., Zickler, T., Belhumeur, P.N., Kriegman, D.J.: Specularity removal in images and videos: A pde approach. In: ECCV (1). (2006) 550–563
16. Tan, R.T., Ikeuchi, K.: Separating reflection components of textured surfaces using a single image. IEEE Trans. Pattern Anal. Mach. Intell. **27** (2005) 178–193
17. Yang, Q., Wang, S., Ahuja, N.: Real-time specular highlight removal using bilateral filtering. In: ECCV (4). (2010) 87–100
18. Yoon, K.J., Choi, Y., Kweon, I.S.: Fast separation of reflection components using a specularity-invariant image representation. In: ICIP. (2006) 973–976
19. Shen, H.L., Zhang, H.G., Shao, S.J., Xin, J.H.: Chromaticity-based separation of reflection components in a single image. Pattern Recognition **41** (2008) 2461–2469
20. Shen, H.L., Cai, Q.Y.: Simple and efficient method for specularity removal in an image. Applied Optics (**48**)
21. Tan, R., Nishino, K., Ikeuchi, K.: Color constancy through inverse intensity chromaticity space. JOSA **21** (2004) 321–334
22. Gonzalez, R.C., Woods, R.E.: Digital image processing. Addison-Wesley (1992)
23. Hojjatoleslami, S.A., Kittler, J.: Region growing: a new approach. IEEE Transactions on Image Processing **7** (1998) 1079–1084
24. PHARR, M., HUMPHREYS, G.: Physically Based Rendering: From Theory to Implementation, 2nd ed. Morgan Kaufmann (2010)